Journal of Controlled Release 385 (2025) 114003

Contents lists available at ScienceDirect

Journal of Controlled Release

journal homepage: www.elsevier.com/locate/jconrel

Oncolytic microgels with regulated antibody release augment tumor immunotherapy

Jiakun Guo [1], Hujing Tan [1], Wanting Chen, Yan Wang, Wenhai Lin, Zhiyuan Zhong [*], Chao Deng [*]

Biomedical Polymers Laboratory, and Jiangsu Key Laboratory of Advanced Functional Polymer Materials, College of Chemistry, Chemical Engineering and Materials Science, and State Key Laboratory of Radiation Medicine and Protection, Soochow University, Suzhou 215123, China

ARTICLE INFO

Keywords:
Cancer immunotherapy
Oncolytic peptide
Immune checkpoint inhibitor
Microparticle
Controlled release

ABSTRACT

The inhibition of immune checkpoints has emerged as a most successful immunotherapy strategy for cancers; however, it bears a modest clinical response rate and certain cases severe systemic adverse reactions. Here, oncolytic microgels (OMG) that possess similar antitumor activity and immune activation to oncolytic peptide LTX-315 and are capable of sustained release of immune checkpoint inhibitors have been developed to potentiate cancer immunotherapy. Of note, antibodies including anti-PD-1, anti-PD-L1, and anti-CTLA-4 all could be quantitatively loaded into OMG while being gradually released over a couple of weeks in vitro and in tumor as well. In the B16F10 melanoma model, a single tumoral injection of anti-PD-1 and anti-CTLA-4-loaded OMG (P1C4@OMG) effectively reversed suppressive tumor microenvironment and enhanced anti-tumor immune response, achieving potent tumor suppression and striking survival benefits. This study heralds oncolytic microgels with regulated antibody release as a safe and unique platform for cancer immunotherapy.

1. Introduction

Cancer immunotherapy involving repression of immune checkpoints, activation of immunostimulatory cascades, and reprogramming immune cells has emerged as a prominent modality to treat malignancies across a broad range of indications [1–3]. The inhibition of immune checkpoints including cytotoxic T lymphocyte antigen 4 (CTLA-4), programmed cell death 1 (PD-1), and programmed cell death 1 ligand 1 (PD-L1) with antibodies is among the most successful immunotherapeutic strategies [4,5]. It is noted, however, that immune checkpoint blockade (ICB) generally requires multiple intravenous administrations of antibodies, which might induce overactivation of immune system, resulting in severe side effects that in some cases cause patient death [6,7]. The safety of ICB therapy might be improved by localregional release of antibodies [8,9].

The ICB therapy is further associated with a modest clinical response rate, which is related to immunosuppressive tumor microenvironment (TME) [10–12]. The chemotherapy, radiotherapy, immune adjuvants, and cancer vaccines that are able to modulate TME have been shown to improve the ICB therapy to varying degrees [13–15]. Oncolytic peptides and polymers capable of directly lysing tumor cells, inducing immunogenic cell death (ICD), and activating dendritic cells provide a potent immunotherapy strategy [16–19]. Compared to oncolytic polymers that are in their infancy and have not yet progressed to clinical testing, the oncolytic peptides with defined structure and sequence have demonstrated promising clinical efficacy in treating advanced melanoma and sarcoma patients [20,21], representing a more advanced approach in cancer immunotherapy. Unfortunately, oncolytic peptides might putrefy the injection site and cause severe systemic toxic effects [22,23]. The nanoformulation of oncolytic peptides has been shown to improve their anti-tumor efficacy, immune activation, and safety [24–27]. Meanwhile, local delivery vehicles including hydrogels and microgels with remarkable biocompatibility, durable and controlled drug release profiles have been recognized as attractive platforms for the site-directed administration of therapeutic peptides and proteins [28,29].

In this study, we have developed oncolytic microgels (OMG) that possess similar antitumor activity and immune activation to oncolytic peptide LTX-315 and are capable of sustained release of immune checkpoint inhibitors (ICIs) to potentiate cancer immunotherapy (Scheme 1). MG fabricated from hyaluronic acid (HA) derivatives via

* Corresponding authors.
E-mail addresses: zyzhong@suda.edu.cn (Z. Zhong), cdeng@suda.edu.cn (C. Deng).
[1] These authors contributed equally to this work.

https://doi.org/10.1016/j.jconrel.2025.114003
Received 1 February 2025; Received in revised form 27 June 2025; Accepted 2 July 2025
Available online 3 July 2025

microfluidic and free radical polymerization techniques were expected to have excellent biodegradability and uniform sizes [30–32]. Taking advantage of strong ionic and hydrogen bonds between drugs and HA, ICIs-loaded OMG (ICI@OMG) was constructed by simply mixing immune checkpoint antibodies with MG, followed by coating with an oncolytic LTX-315 peptide. The robust LTX-315 coating on MG would facilely manipulate of the loading capacity and release profiles of encapsulated antibodies. In mice bearing B16F10 melanoma, a single intratumoral (i.t.) administration of anti-PD-1 and anti-CTLA-4-loaded MG (P1C4@OMG) effectively promoted the infiltration of $CD8^+$ and $CD4^+$ T cells as well as the secretion of pro-inflammatory cytokines, significantly suppressed the tumor growth, and remarkably extended the survival time, without causing obvious side effects and dysfunction.

2. Experimental section

2.1. Materials

Hyaluronic acid (HA, molecular weight: 9.0 kDa and 36 kDa) was purchased from Freda Biopharm Co. Ltd. 2-Aminoethyl methacrylate hydrochloride (AMA) and 4-(4,6-dimethoxy-1,3,5-triazin-2-yl)-4-methylmorpholin-4-ium chloride (DMTMM) were purchased from Macklin. Anti-mouse CTLA-4 (clone: 9D9), anti-mouse PD-1 (clone: RMP1–14), and anti-mouse PD-L1 (clone: 10F.9G2™) were purchased from Bioxcell. LTX-315 peptide (KKWWKKW(*Dip*)K-NH_2, 98 %) was purchased from Chinapeptides. Dimethyl sulfoxide (DMSO) was bought from Sinopharm Chemical Reagent Co., LTD. Micro BCA™ protein assay kit was obtained from Thermo Fisher Scientific. Cy5-NHS ester, sulfo-Cy7-NHS ester, and sulfo-Cy3-NH_2 were provided by Dalian Meilun Biotech Co., Ltd. Mouse IL-6, TNF-α, IL-12p70, and IL-10 ELISA kits were purchased from Thermo Fisher Scientific. Recombinant mouse granulocyte-macrophage colony-stimulating factor (GM-CSF) was provided by Peprotech. Anti-calreticulin (αCRT, Proteintech, Cat. 10292–1-AP), anti-heat shock protein 70 (αHSP70, Proteintech, Cat. 10995–1-AP), and anti-high mobility group box-1 protein (αHMGB1, Proteintech, Cat. 10,829–1-AP) antibodies were used directly after purchase.

2.2. Preparation of microgels

Microgels (MG) were prepared from HA-AMA via microfluidic and photo-controlled free radical polymerization techniques. HA-AMA at a concentration of 100 mg/mL and I2959 at a concentration of 6 mg/mL in phosphate buffer (PB) solution (pH 8.5, 10 mM) was loaded into the syringe as the water phase of the microfluidic device, and mineral oil with 10 wt% Span 80 was loaded as the oil phase. Then, the microdroplets were formed by hydrodynamically shearing the core flow of water phase in a microchannel by the lateral oil phase and then photo-crosslinked under UV irradiation at 365 nm to obtain MG. Excessive PB, isopropyl alcohol, and n-hexane were used to remove the mineral oil, Span 80, and I2959 initiator.

2.3. Loading of antibodies and LTX-315

Antibodies were encapsulated into MG by dialysis replacement. For single antibody loading, 150 μL of antibody solution (1.2–5.2 mg/mL) in PBS (pH 7.4, 10 mM) was added to 300 μL of MG suspension (30 mg/mL). Then, the mixture was dialyzed six times using PB solution (pH 5.0), with the dialysis medium refreshed every hour. The unloaded antibodies in the supernatant solution were detected using the bicinchoninic acid (BCA) protein assay kit. The drug loading efficiency (DLE) and drug loading content (DLC) were calculated according to the following formulations. IgG protein was similarly loaded in MG except that the theoretical DLC was set at 2–8 wt%. The co-loading of dual antibodies (anti-CTLA-4 and anti-PD-1) in MG was performed by initially adding the two antibody solution in PBS (150 μL) into 300 μL of MG suspension (30 mg/mL), followed by a similar protocol to single antibody loading.

$$\mathrm{DLC\,(wt\%)} = \mathrm{Weight\ of\ drug\ loaded / Weight\ of\ drug\ and\ microgels} \times 100$$

$$\mathrm{DLE\,(\%)} = \mathrm{Weight\ of\ drug\ encapsulated / Total\ weight\ of\ drug\ used} \times 100$$

LTX-315 was encapsulated in MG by simply mixing LTX-315 with MG in aqueous solution to obtain OMG. Briefly, an MG suspension (25 mg/mL) was mixed with an equivalent volume of LTX-315 solution at a theoretical DLC of 10–30 wt%. At predetermined time points, the

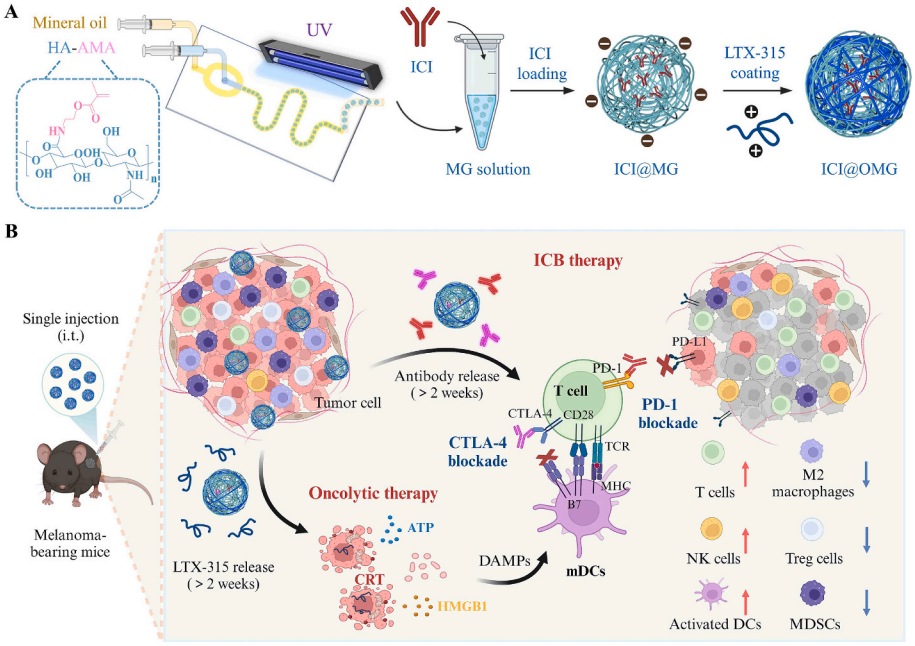

Scheme 1. Schematic illustration of oncolytic microgels (OMG) with regulated antibody release to augment tumor immunotherapy. OMG with antitumor activity and immune activation comparable to oncolytic peptide LTX-315 are capable of sustained release of immune checkpoint inhibitors (ICIs) to orchestrate oncolytic therapy and cancer immunotherapy.

unloaded LTX-315 in the supernatant was measured via an ultraviolet spectrophotometer. DLE and DLC of LTX-315 were similarly calculated. In the same way, ICI@OMG and IgG@OMG were prepared by mixing ICI@MG with LTX-315.

2.4. In vitro drug release of IgG and LTX-315

In vitro release of Cy3-labeled IgG (Cy3-IgG) and LTX-315 from IgG@OMG was carried out in PBS (pH 6.5, 10 mM). Briefly, 100 μL of IgG@OMG (25 mg/mL MG) was placed in the insert of transwell plates. Then, 1.0 mL of PBS was added to the plates to immerse IgG@OMG. The plates were placed on a shaking table at 37 °C and 100 rpm. At predetermined time points, the release medium was collected and refreshed with PBS (1.0 mL). The amount of Cy3-IgG and LTX-315 in the release medium was measured with a multifunctional microplate reader and an ultraviolet spectrophotometer, respectively.

2.5. Immunogenic cell death (ICD) of B16F10 cells induced by OMG

After inoculating in 6-well plates for 12 h, B16F10 cells (2×10^5/cell) were treated with free LTX-315 or OMG (LTX-315: 20 μg/mL) for 24 h. The supernatant was collected for adenosine triphosphate (ATP) and HMGB1 determination. The cells were digested with pancreatic enzymes, washed twice with PBS, stained with αCRT and Alexa Fluor 647-labeled secondary antibodies for 1 h and 30 min, respectively. CRT expression on the B16F10 cell surface was detected via flow cytometry. HSP70 expression was similarly determined except that αHSP70 was used.

In order to observe the CRT and HMGB1 expression using confocal imaging, B16F10 cancer cells were allowed to attach to 18 mm glass cover slides in 12-well plates for 12 h, and then treated with PBS, free LTX-315, or OMG for 24 h. After fixing with 4 % paraformaldehyde at room temperature for 15 min, the cells were incubated with αCRT or αHMGB1 antibodies overnight, and then stained with Alexa Fluor 647 conjugated secondary antibodies for 1 h. The stained cells were mounted on a slide and imaged via confocal microscopy.

2.6. Tumor retention of IgG@OMG

B16F10 tumor model was established by subcutaneous injection of B16F10 cells (1×10^5 cells, 50 μL) on the right hind flank of mice (C57BL/6 J, female, 6–8 weeks, 18–20 g). Cy5-labeled LTX-315 (Cy5-LTX-315) and Cy7-labeled rat IgG (Cy7-IgG) were used to monitor the retention of antibodies and peptides following the intratumoral administration. Mice treated with LTX-315, IgG, or IgG@OMG were imaged via an in vivo fluorescence imaging system (PerkinElmer IVIS Lumina III) at different time points, and the drug retention was quantified by measuring the corresponding fluorescence densities.

2.7. In vivo tumor therapy

All the animal experiments were approved by the Animal Care and Use Committee of Soochow University, and all the protocols conformed to the Guide for the Care and Use of Laboratory Animals. The in vivo antitumor effect of anti-CTLA-4-loaded microgels (C4@MG) was assessed in subcutaneous B16F10 melanoma. After 10 days, the tumors (50–100 mm^3) were treated with a single i.t. administration (50 μL) of free anti-CTLA-4 (4 mg/kg), C4@MG (2 mg/kg), C4@MG (4 mg/kg), or C4@MG (8 mg/kg), and 4 doses of i.v. injection (50 μL) of anti-CTLA-4 (1 mg/kg) on days 0, 2, 4, and 6. The tumor volume was measured and calculated as follows: tumor volume = $\text{width}^2 \times \text{length} \times 0.5$. The weights of the mice were recorded every other day. Mice were considered to have reached the endpoint of the study if they died, lost more than 15 % of their initial body weight, or if the tumor volume reached 1500 mm^3 during treatment.

To evaluate the therapeutic efficacy of LTX-315 peptide-coated C4@MG (C4@OMG), 50 μL of free drug (anti-CTLA-4 and LTX-315), OMG, C4@MG, or C4@OMG was i.t. injected on day 0. The dosages of LTX-315 and anti-CTLA-4 were 45 mg/kg and 4 mg/kg, respectively. To assess the therapeutic efficacy of MG loaded with LTX-315, anti-CTLA-4, and anti-PD-1 (P1C4@OMG), 50 μL of free drug (anti-CTLA-4 and anti-PD-1), OMG, P1C4@MG, or P1C4@OMG was injected into the tumor on day 0. The dosages of LTX-315, anti-CTLA-4, and anti-PD-1 were 45 mg/kg, 4 mg/kg, and 4 mg/kg, respectively.

2.8. Statistical data analysis

Statistical analysis was performed by GraphPad Prism software 9.0. All data in this paper were presented as mean ± SD. Statistical differences between multiple groups were analyzed by one-way ANOVA, and the statistical analysis of mouse survival was performed by the log-rank (Mantel-Cox) test. p values: $^*p < 0.05$, $^{**}p < 0.01$, $^{***}p < 0.001$, and $^{****}p < 0.0001$.

3. Results and discussion

3.1. Microgel construction and antibody loading

MG was constructed from HA derivatives via microfluidic and free radical polymerization techniques. Considering that lower molecular weight HA facilitates the preparation of polymer solutions with reduced viscosity at equivalent concentrations, which is critical for achieving precise microgel fabrication through microfluidic technique at elevated polymer concentrations and enhanced drug loading capacity (Fig. S1), HA with a low molecular weight of 9.0 kDa was employed to develop HA derivatives for microgel construction. By adjusting the flow rate ratios between aqueous and oil phases (1:3 to 1:5), MG with sizes ranging from 60 to 120 μm was successfully fabricated (Fig. S2). The formed MG presented uniform sizes, narrow distribution (CV < 3.0 %), and spherical morphology (Figs. 1A, S2). Different antibodies could be facilely loaded into MG by directly mixing with the preformed MG, and an increasing antibody loading capacity was observed with decreasing pH from 7.4 to 5.0 (Fig. S3). At pH 5.0, the larger counterparts (90 and 120 μm) exhibited a high DLE exceeding 90 % compared to relatively low protein encapsulation efficiency of 60 μm MG (Fig. S4) likely owing to enhanced pore accessibility. For 90 μm MG, over 95 % DLE was achieved at pH 5.0 for anti-PD-1, anti-PD-L1, and anti-CTLA-4 antibodies at a theoretical drug loading content (DLC) of 5 wt% as the result from the strong electrostatic and hydrogen bonding interactions between MG and antibodies (Fig. 1B). Meanwhile, nearly quantitative loading of positively charged LTX-315 in 90 μm MG was obtained within five minutes even when the theoretical DLC increased to 30 wt% (Figs. 1C, S5). Based on the drug loading capacity and microgel injectability performance, 90 μm MG was selected for subsequent studies. Following the coating with varying amounts of LTX-315, IgG-loaded MG displayed superior loading capacity (Figs. 1D, S6). Confocal imaging revealed that Cy7-IgG was evenly distributed in MG, while the Cy5-LTX-315 was mainly located in the outer layer of MG (Fig. 1E), signifying the successful antibody loading and peptide coating. MG following the encapsulation of IgG and LTX-315 demonstrated analogous sizes and morphology (Fig. 1F). Notably, IgG@OMG exhibited exceptional storage stability at 4 °C, with less than 1 % drug leakage for both IgG and LTX-315 over 28 days (Fig. S7). Similarly, MG loaded with both anti-CTLA-4 and anti-PD-1 (P1C4@OMG) was prepared by mixing the two antibodies with MG suspension followed by dialysis. In order to achieve the same loading content of both antibodies in P1C4@OMG, we adjusted their theoretical loading contents and found that 5.0 wt% DLC was achieved when the theoretical DLC of anti-CTLA-4 and anti-PD-1 was set at 5.2 wt% and 5.45 wt%, respectively (Table S1).

In contrast with a burst IgG release (approximately 60 % release in one day) from MG without LTX-315 coating, MG coated with LTX-315 presented sustained release of both antibodies and LTX-315 (Fig. 1G).

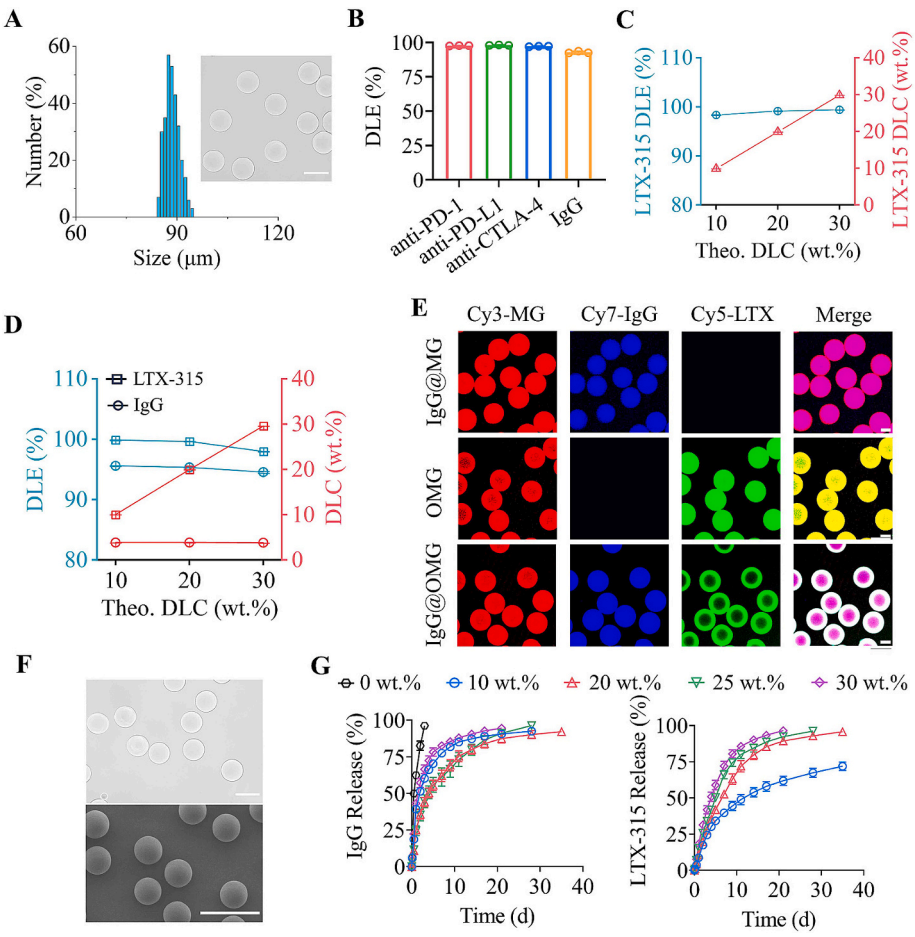

Fig. 1. Loading and controlled release of ICI antibodies in MG with an average diameter of 90 μm. (A) Size and size distribution of MG determined by microscopy (n = 300). Inset: microscopy image. (B) DLE of anti-PD-1, anti-PD-L1, anti-CTLA-4, and IgG in MG at pH 5.0 at a theoretical DLC of 5 wt% (n = 3). (C) DLE and DLC of LTX-315 in OMG at theoretical DLC of 10–30 wt% (n = 3). (D) Effect of LTX-315 on drug loading, the theoretical DLC of IgG was fixed at 5 wt% (n = 3). (E) Confocal laser scanning microscopy (CLSM) images of IgG@MG, OMG, and IgG@OMG. MG, IgG, and LTX-315 were labeled with Cy3, Cy7, and Cy5, respectively. (F) Size distribution and morphology of IgG@OMG observed by microscopy (top) and scanning electron microscopy (bottom). (G) In vitro release curves of IgG and LTX-315 from IgG@OMG in PBS solution (pH 6.5, 150 mM NaCl) (n = 3). Scale bars: 100 μm. Data are presented as mean ± SD.

Increasing LTX-315 loading content from 0 to 25 wt% prolonged the antibody release up to four weeks, while further elevation the LTX-315 loading content induced faster IgG release possibly due to that excessive LTX-315 compromises the interactions of antibodies with MG. Thus, MG coated with 25 wt% exquisitely balancing the drug loading capacity and long-term drug release was employed for the following studies. Notably, the release of the antibody and LTX-315 was significantly accelerated in the presence of sodium chloride (NaCl) (Fig. S8), indicating that the disruption of electrostatic interactions plays a critical role in the drug release.

3.2. *In vitro antitumor efficacy and immunoactivation*

MG induced little cytotoxicity with cell viability of over 95 % in both L929 normal and B16F10 tumor cells after 48 h incubation at MG concentration up to 1.0 mg/mL (Fig. S9), signifying the good biocompatibility of MG. Similar to free oncolytic LTX-315 peptide, OMG caused equivalent cytotoxicity with a half-maximal inhibitory concentration (IC_{50}) of 19.30 μg/mL and noticeable apoptosis in B16F10 cells (Fig. 2A–C). The comparable cytotoxicity between OMG and free LTX-315 was primarily attributed to the presence of NaCl in the cell culture media as well as extensive dilution, resulting in approximately 85 % of LTX-315 release from OMG within 24 h (Fig. S10). In normal cells (L929 fibroblasts) and other cancer cells (4T1 cells), OMG also displayed similar cytotoxicity compared to free LTX-315 (Fig. S11). CLSM images revealed that B16F10 cells treated with OMG for 24 h presented apparent expression of CRT and marked decrease of HMGB1 signal owing to the escape of HMGB1 from the nucleus when cells were dying. Quantitative analysis showed that OMG caused approximately 2.5 times higher expression of CRT and HSP70 as well as significantly elevation of the extracellular ATP and HMGB1 expression levels (Fig. 2E). These results suggested that OMG produced a remarkable release of damage associated molecular patterns (DAMPs), which might serve as tumor associated antigens (TAAs) for initiating the immune response via antigen presenting cells (APCs) [33–36]. Indeed, the DAMP released from B16F10 cells induced around 20 % activation of bone marrow-derived dendritic cells (BMDCs), which was 7.7 times higher than PBS group (Fig. 2F,G). In the supernatant of BMDCs, OMG group revealed over 3 times higher secretion levels of immunostimulatory factors interlukin-6 (IL-6), tumor necrosis factor-α (TNF-α), and IL-12p70 (Fig. 2H–J), and significantly lower levels of immunosuppressive factors like IL-10 than PBS group (Fig. 2K), corroborating that strong immunoactivation was initiated by OMG.

3.3. *Tumor accumulation and in vivo antitumor efficacy*

Cy7-IgG and Cy5-LTX-315 were employed to evaluate their tumor accumulation. Following i.t. injection, free IgG and LTX-315 showed a rapid elimination, and IgG and LTX-315 fluorescence signal was invisible after 2 d administration (Figs. 3A,B). On the contrary, MG enabled

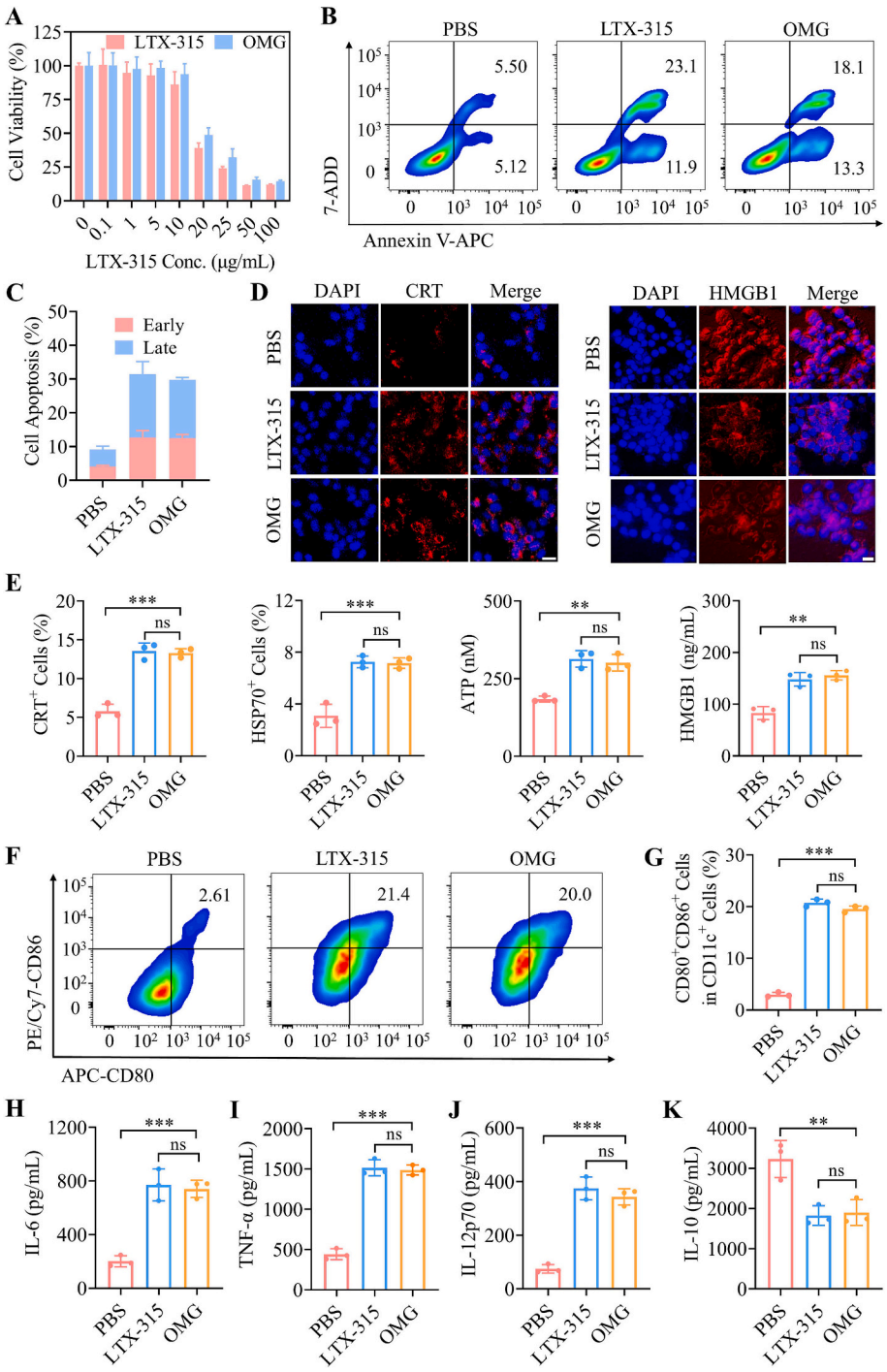

Fig. 2. In vitro evaluation of the anti-tumor effect and immunostimulatory capacity of OMG. (A) Cytotoxicity of OMG toward B16F10 cells after 48 h incubation (n = 6). (B) Apoptosis of B16F10 cells after 48 h treatment. (C) Quantitative analysis of cell apoptosis (n = 3). (D) CLSM images of B16F10 cells stained with APC-labeled CRT antibody and HMGB1 antibody after 24 h incubation with PBS, free LTX-315, and OMG. (E) Levels of CRT, HSP70, ATP, and HMGB1 in B16F10 cells after 24 h treatment (n = 3). (F) Representative flow cytometry graphs for the expression of CD80 and CD86 by BMDCs. (G) Quantification of $CD80^+CD86^+$ BMDCs in $CD11c^+$ cells (n = 3). (H) IL-6, (I) TNF-α, (J) IL-12p70, and (K) IL-10 concentrations released from BMDCs treated with different formulations for 24 h (n = 3). For B—K, the LTX-315 concentration was 20 μg/mL. Data are presented as mean ± SD, and p values were calculated via one-way ANOVA test. ns > 0.05; *p < 0.05; **p < 0.01; ***p < 0.001; ****p < 0.0001.

much longer tumor retention of IgG and LTX-315, in which approximately 75.1 % of IgG and 55.9 % of LTX-315 were detected at tumor sites on day one and their enrichment persisted for over 14 d. The higher retention for drugs in MG can be primarily attributed to that covalently cross-linked MG with a diameter of 90 μm has difficulty diffusing through capillaries or the lymphatic system, and is prone to form a reservoir for sustained drug release at the injection site. The long-term accumulation of antitumor therapeutics at the tumor sites often reduces the required dosages and provides a sustained superior therapeutic effect [37–40].

Given that both LTX-315 and ICIs have been frequently employed in clinical trials and treatment of melanoma patients [41,42], B16F10 subcutaneous tumor model (around 75 mm^3) was established to evaluate the in vivo therapeutic efficacy (Fig. 3C). In clinical and preclinical

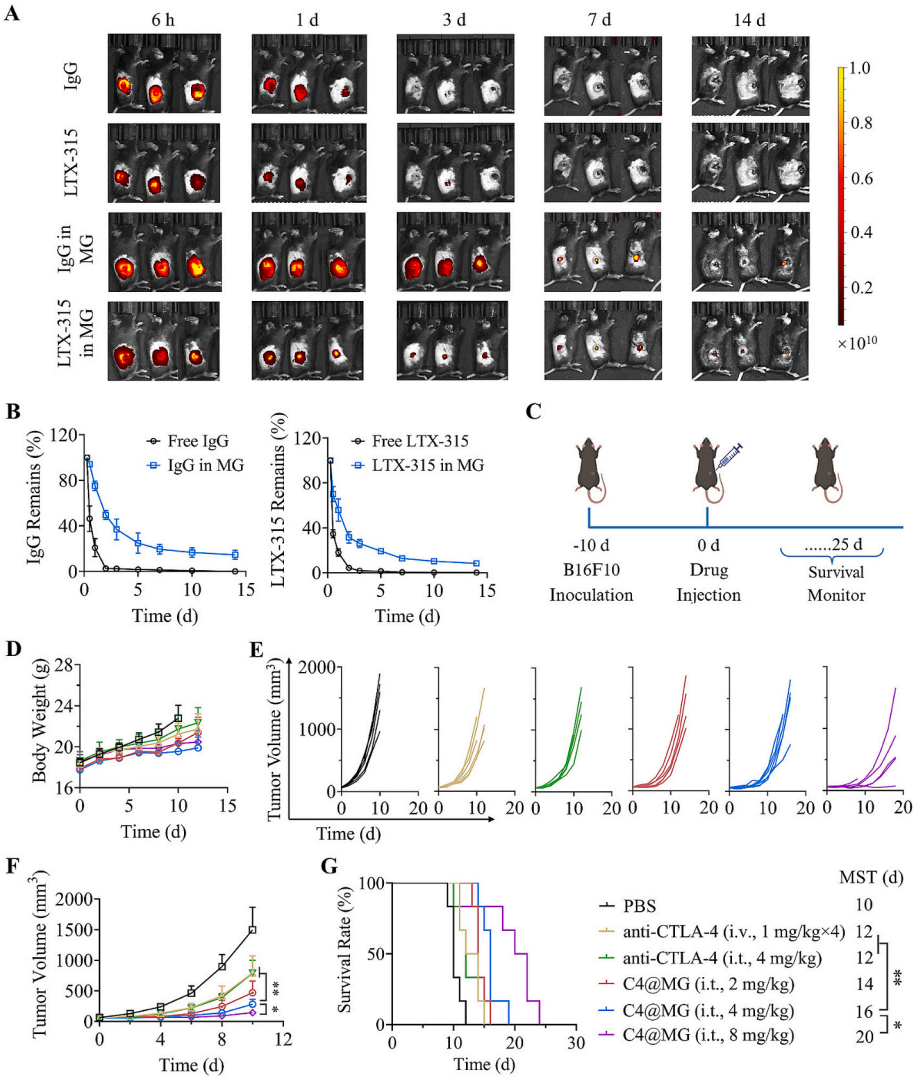

Fig. 3. Tumor retention and in vivo therapeutic efficacy in B16F10 tumor-bearing mice. (A) IVIS imaging of mice i.t. administered with free LTX-315, IgG, and IgG@OMG ($n = 3$). LTX-315 and IgG were stained with Cy5 and Cy7, respectively. (B) Semi-quantitative analysis of the retention of IgG and LTX-315 (n = 3). (C) Diagram for the establishment, treatment, and monitoring of B16F10 melanoma mouse model. (D) Body weight curves. (E) Individual tumor growth curves. (F) Average tumor growth curves. (G) Survival curves. D–G, $n = 6$. Data are presented as mean ± SD, and p values were calculated via one-way ANOVA test. ns > 0.05; $^{*}p < 0.05$; $^{**}p < 0.01$; $^{***}p < 0.001$; $^{****}p < 0.0001$.

studies, ICIs are generally administered through multiple i.v. injections [43,44]. Thus, the therapeutic outcomes and safety were assessed by comparing a single i.t. administration of murine ICI@MG with four i.v. injections of ICIs. Importantly, MG loaded with anti-CTLA-4 (C4@MG) at dosages of 2–8 mg/kg of anti-CTLA-4 caused no body weight loss, corroborating the excellent safety (Fig. 3D). In comparison with four doses of i.v. administration and one dose of i.t. administration of free anti-CTLA-4, a single i.t. injection of C4@MG displayed better tumor inhibition and survival rate at 4 mg/kg of anti-CTLA-4 (Fig. 3E,F). All mice in PBS group died within 12 days owing to aggressive tumor growth (Fig. 3G). In contrast, C4@OMG significantly extended the survival time as a result from effective tumor suppression. Moreover, increasing the dosage of anti-CTLA-4 in MG to 8 mg/kg largely improved the tumor suppression and extended the survival rate with a median survival time (MST) of 20 days (Fig. 3G). Although 8 mg/kg of anti-CTLA-4 showed the best antitumor effect, toxic side effects including constipation and fur loss were observed during treatment. Therefore, 4 mg/kg of anti-CTLA-4 was selected for the following studies.

Taking advantages of oncolytic effect and ICD generation, LTX-315 peptide was coated on C4@MG (C4@OMG) to manipulate the antibody release and orchestrate oncolytic therapy and cancer immunotherapy (Fig. 4A). Cancer combination therapy by selecting rational agents and combinations often affords superior therapeutic outcomes [45–49]. Both C4@OMG and OMG resulted in a gradual increase in body weight over time (Fig. 4B), indicating that MG local delivery system could largely increase the safety and therapeutic windows of oncolytic peptides and ICIs. In contrast, free anti-CTLA-4 and LTX-315 induce significant body weight loss of mice possibly owing to the overactivation of systemic immunity and excessive toxicity toward healthy tissues [50–52]. Notably, C4@OMG displayed nearly complete tumor inhibition within 14 days, in sharp contrast to rapid tumor growth in other groups (Fig. 4C,D). Consistently, mice treated with C4@OMG displayed a significantly extended survival rate with an MST of 28 d, which was much longer than that in OMG and C4@MG groups (Fig. 4E). The improved therapeutic outcomes could attribute to the coordination of immune checkpoint blockade by anti-CTLA-4 with oncolytic and ICD effect of LTX-315. Meanwhile, the elevation of CTLA-4 expression on $CD8^{+}$ T cells in the tumor, lymph nodes, spleen, and peripheral blood induced by LTX-315 was reversed by anti-CTLA-4 (Figs. 4F,G, S12), indicating the significance of combination therapy.

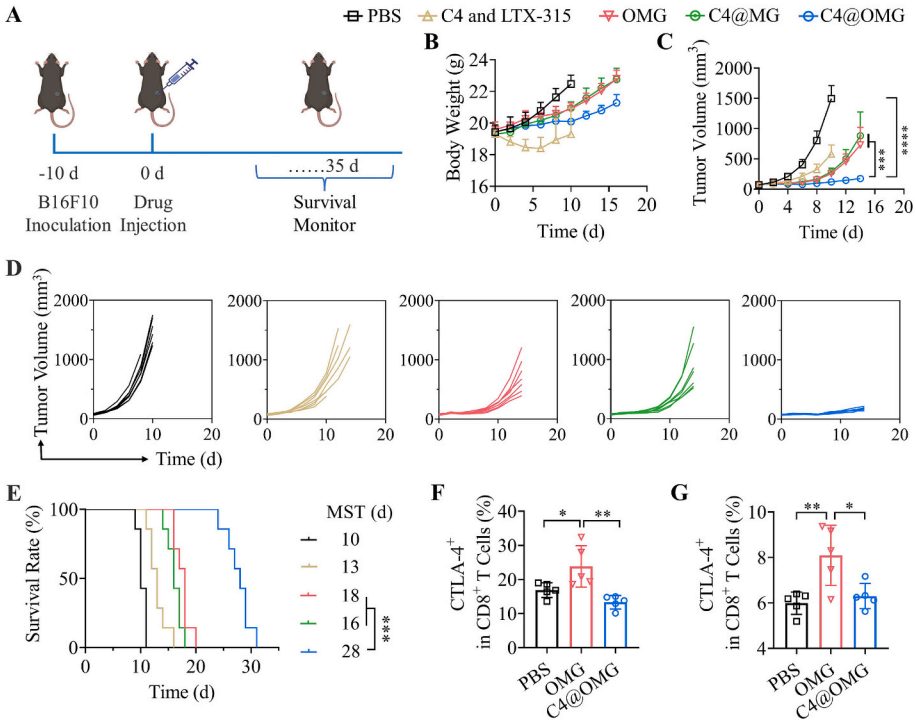

Fig. 4. In vivo therapeutic effect of C4@OMG in B16F10 tumor-bearing mice. (A) Diagram for the establishment, treatment, and monitoring of the B16F10 mouse model. The mice were received i.t. injections of PBS, C4, and LTX-315, OMG, C4@MG, and C4@OMG on day 0. The doses of LTX-315 and C4 were 45 mg/kg and 4 mg/kg, respectively. (B) Body weight curves of mice over time. (C) Average tumor growth curves. (D) Individual tumor growth curves. (E) Survival curves. B–E, $n = 7$. CTLA-4 expression on $CD8^+$ T cells in the tumor (F) and lymph nodes (G) after i.t. injection of PBS, OMG, and C4@OMG ($n = 5$). The doses of LTX-315 and C4 were 45 mg/kg and 4 mg/kg, respectively. Data are presented as mean ± SD, and p values were calculated via one-way ANOVA test. ns > 0.05; $^*p < 0.05$; $^{**}p < 0.01$; $^{***}p < 0.001$; $^{****}p < 0.0001$.

Moreover, MG could accomplish robust co-loading of multiple ICIs and peptides. In clinic, anti-PD-1 is mostly recommended to combine with anti-CTLA-4 for the treatment of melanoma [53]. Thus, P1C4@OMG loading with anti-PD-1 and anti-CTLA-4 was constructed and employed to treat B16F10 melanoma (Fig. 5A). Notably, intratumoral injection of anti-PD-1 at a dose of 2–10 mg/kg or intravenous administration at 1 mg/kg for three to four doses has been typically utilized in previous murine tumor studies [54–58]. Thus, a single intratumoral injection of P1C4@OMG with 4 mg/kg of anti-PD-1 was employed for in vivo anticancer efficacy evaluation. Mice treated with P1C4@OMG showed slight tumor growth within 20 d, in sharp contrast to the fast increase of tumor volumes in OMG and P1C4@MG groups (Fig. 5B,C). Furthermore, P1C4@OMG resulted in the significant extension of survival time with an MST of 35 d and 1/7 tumor free (Fig. 5D). During the whole experimental period, P1C4@OMG caused gradual increase of body weight (Fig. 5E). Different from the significant increase of serum alanine aminotransferase (ALT), aspartate aminotransferase (AST), urea (UREA), and creatinine (CREA) levels of mice injected with free anti-PD-1 and anti-CTLA-4, P1C4@OMG group presented similar blood biochemical indexes to those of normal mice (Fig. S13). In addition, the P1C4@OMG caused little influence on the total numbers of red blood cells (RBC), hemoglobin (HGB), and red blood cell backlog (HCT) in the blood of mice, while mice treated with free anti-PD-1 and anti-CTLA-4 showed significantly reduced levels (Fig. S14). Histological analysis revealed that no detectable damage to major organs was caused by OMG, P1C4@MG, and P1C4@OMG (Fig. S15). These results suggested that the introduction of MG delivery system could avoid the risk of anemia and the hepatorenal dysfunction induced by free immune checkpoint inhibitors, and largely broaden their therapeutic window.

Owing to the generated DAMPs and tumor-specific antigen, LTX-315-bearing formulation (OMG) induced significant increase of mature DCs ($CD11c^+CD80^+CD86^+$) in lymph nodes (LNs), which was further increased by adding ICIs (Fig. 5F). Comparing to the slight increase of $CD4^+$ T, $CD8^+$ T, and NK cells in the tumors treated by free anti-CTLA-4 and anti-PD-1, ICIs-loaded in MG (P1C4@MG) induced approximately two-fold increase in the infiltration of these cells (Fig. 5G–I), highlighting the critical role of long-acting delivery of ICIs. The infiltration of the cytotoxic T and NK cells was further increased by the introduction of LTX-315 (P1C4@OMG). Moreover, both OMG and P1C4@MG significantly reduced the proportions of immunosuppressive cells including M2 macrophages, MDSCs, and Treg in tumors, in contrast to a slight change of immunosuppressive cells in free ICI group (Fig. 5J–L). Additionally, P1C4@OMG induced 2.1-fold higher CTLs/Tregs ratio in the tumors compared to the LTX-315-free counterpart (P1C4@MG) (Fig. S16). In the spleens, P1C4@OMG group also presented the most infiltration of $CD8^+$ effector T cells and $CD4^+$ helper T cells (Figs. 5M, S17). Similarly, P1C4@MG generated more IFN-γ^+CD8^+, IFN-γ^+CD4^+, TNF-α^+CD8^+, and TNF-α^+CD4^+ T cells in spleens than the free counterparts, which could be significantly increased by the incorporation of LTX-315 (Fig. 5N–Q). Thus, MG provides ICIs and oncolytic peptides with apparent activation of DCs, remarkable elevation of the infiltration of cytotoxicity T and NK cells, and significant downregulation of immunosuppressive cells, achieving long-acting activation of immune response and potent antitumor efficacy.

4. Conclusion

We have demonstrated that oncolytic microgels (OMG) could achieve localregional long-acting co-delivery of oncolytic peptides and antibodies targeting immune checkpoints to potentiate cancer immunotherapy. Taking advantages of strong ionic and hydrogen bonds between drugs and microgels, ICI@OMG afforded quantitative loading of different ICI antibodies (anti-PD-1, anti-PD-L1, and anti-CTLA-4), and

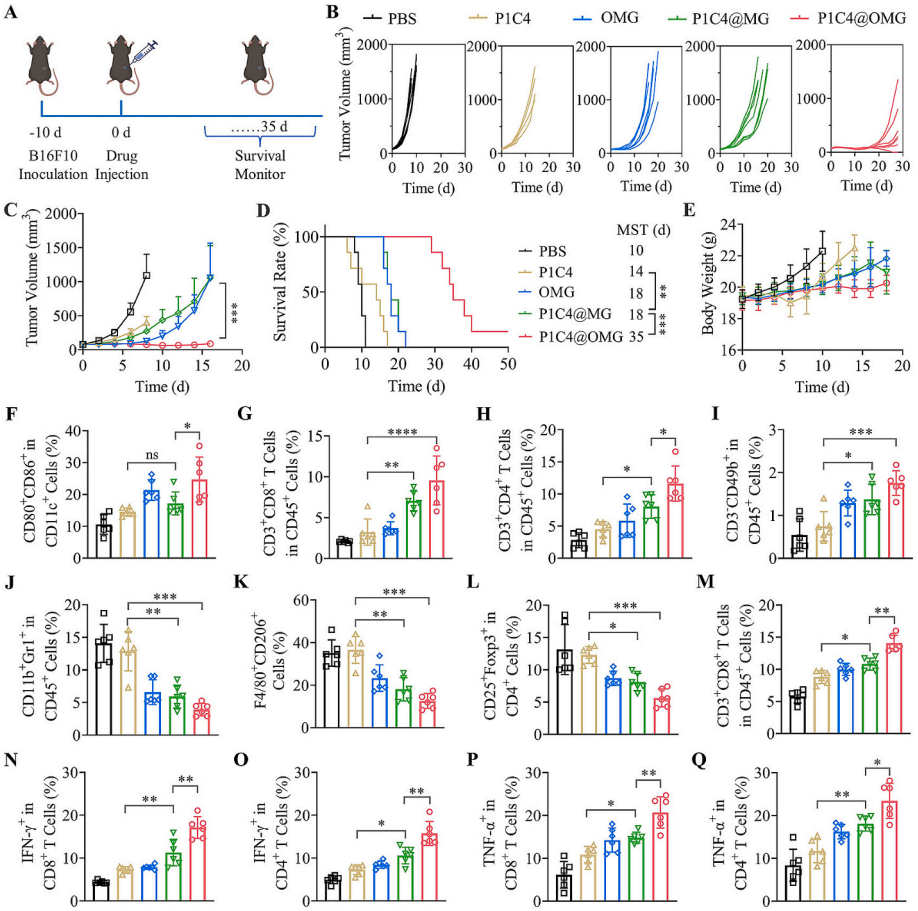

Fig. 5. In vivo therapeutic effect of P1C4@OMG in B16F10 tumor-bearing mice. (A) Diagram for the establishment, treatment, and monitoring of the B16F10 mouse model. The doses of LTX-315, anti-CTLA-4, and anti-PD-1 were 45 mg/kg, 4 mg/kg, and 4 mg/kg, respectively. (B) Individual tumor growth curves. (C) Average tumor growth curves. (D) Survival curves. (E) Body weight. B–E, n = 7. (F–Q) Flow cytometric analysis was performed in B16F10 melanoma-bearing mice 7 days after i.t. injection of PBS, P1C4, OMG, P1C4@MG, and P1C4@OMG. ($n = 6$). The doses of LTX-315, anti-CTLA-4, and anti-PD-1 were 45 mg/kg, 4 mg/kg, and 4 mg/kg, respectively. (F) Quantification of mature DCs in the lymph nodes. Quantification of $CD8^+$ T (G) and $CD4^+$ T (H) cells in the tumor. Quantification of $CD49b^+$ NK cells (I), M2 macrophages (J), MDSCs (K), and Treg (L) in the tumors. (M) Quantification of $CD8^+$ T cells in the spleen. Quantification of IFN-γ^+ expressing $CD8^+$ T cells (N), IFN-γ^+ expressing $CD4^+$ T cells (O), TNF-α^+ expressing $CD8^+$ T cells (P), and TNF-α^+ expressing $CD4^+$ T cells in the spleen (Q). Data are presented as mean ± SD, and p values were calculated via one-way ANOVA test. ns > 0.05; *$p < 0.05$; **$p < 0.01$; ***$p < 0.001$.

long-term tumor retention and sustained release of both antibodies and LTX-315. Notably, MG loaded with anti-CTLA-4 (C4@MG) demonstrated better tumor suppression and prolonged survival compared to free antibodies administered intravenously and intratumoral in B16F10 melanoma-bearing mice. The therapeutic efficacy could be improved by increasing the dosages or introducing LTX-315. In addition, MG could accomplish co-loading of multiple ICIs and peptides, and P1C4@OMG effectively promoted the infiltration of $CD8^+$ and $CD4^+$ T cells as well as the secretion of pro-inflammatory cytokines, affording significantly improved tumor suppression and survival extension with partial tumor free. Compared with the obvious anemia and hepatorenal dysfunction caused by free ICIs, P1C4@OMG presented superior safety with normal blood biochemical and routine indexes. Thus, OMG as a safe and powerful long-acting delivery platform for immune checkpoint antibodies holds tremendous potential to augment cancer immunotherapy.

CRediT authorship contribution statement

Jiakun Guo: Writing – original draft, Methodology, Investigation, Data curation, Conceptualization. **Hujing Tan:** Writing – original draft, Investigation, Data curation. **Wanting Chen:** Methodology, Formal analysis. **Yan Wang:** Investigation. **Wenhai Lin:** Writing – original draft. **Zhiyuan Zhong:** Writing – review & editing, Conceptualization. **Chao Deng:** Writing – review & editing, Supervision, Project administration, Funding acquisition, Conceptualization.

Declaration of competing interest

The authors declare no competing financial interest.

Acknowledgments

This work was financially supported by the National Key Research and Development Program of China (2021YFB3800900) and the National Natural Science Foundation of China (52373299, 51973149).

Appendix A. Supplementary data

Supplementary data to this article can be found online at https://doi.org/10.1016/j.jconrel.2025.114003.

Data availability

Data will be made available on request.

References

[1] A. van Weverwijk, K.E. de Visser, Mechanisms driving the immunoregulatory function of cancer cells, Nat. Rev. Cancer 23 (2023) 193–215.
[2] G. Oliveira, C.J. Wu, Dynamics and specificities of T cells in cancer immunotherapy, Nat. Rev. Cancer 23 (2023) 295–316.
[3] F.G. Dall'Olio, A. Marabelle, C. Caramella, C. Garcia, M. Aldea, N. Chaput, C. Robert, B. Besse, Tumour burden and efficacy of immune-checkpoint inhibitors, Nat. Rev. Clin. Oncol. 19 (2022) 75–90.
[4] S. Bagchi, R. Yuan, E.G. Engleman, Immune checkpoint inhibitors for the treatment of cancer: clinical impact and mechanisms of response and resistance, Annu. Rev. Pathol. 16 (2021) 223–249.
[5] Y. Shiravand, F. Khodadadi, S.M.A. Kashani, S.R. Hosseini-Fard, S. Hosseini, H. Sadeghirad, R. Ladwa, K. O'Byrne, A. Kulasinghe, Immune checkpoint inhibitors in cancer therapy, Curr. Oncol. 29 (2022) 3044–3060.
[6] A.D. Waldman, J.M. Fritz, M.J. Lenardo, A guide to cancer immunotherapy: from T cell basic science to clinical practice, Nat. Rev. Immunol. 20 (2020) 651–668.
[7] Q. Sun, Z. Hong, C. Zhang, L. Wang, Z. Han, D. Ma, Immune checkpoint therapy for solid tumours: clinical dilemmas and future trends, Signal Transduct. Target. Ther. 8 (2023) 320.
[8] J. Kim, D.M. Francis, L.F. Sestito, P.A. Archer, M.P. Manspeaker, M.J. O'Melia, S. N. Thomas, Thermosensitive hydrogel releasing nitric oxide donor and anti-CTLA-4 micelles for anti-tumor immunotherapy, Nat. Commun. 13 (2022) 1479.
[9] T. Fang, X. Cao, B. Shen, Z. Chen, G. Chen, Injectable cold atmospheric plasma-activated immunotherapeutic hydrogel for enhanced cancer treatment, Biomaterials 300 (2023) 122189.
[10] G. Morad, B.A. Helmink, P. Sharma, J.A. Wargo, Hallmarks of response, resistance, and toxicity to immune checkpoint blockade, Cell 184 (2021) 5309–5337.
[11] I. Hirsch, D.A. Goldstein, I.F. Tannock, M.O. Butler, D.C. Gilbert, Optimizing the dose and schedule of immune checkpoint inhibitors in cancer to allow global access, Nat. Med. 28 (2022) 2236–2237.
[12] S. Zhang, Y. Zhang, Y. Feng, J. Wu, Y. Hu, L. Lin, C. Xu, J. Chen, Z. Tang, H. Tian, X. Chen, Biomineralized two-enzyme nanoparticles regulate tumor glycometabolism inducing tumor cell pyroptosis and robust antitumor immunotherapy, Adv. Mater. 34 (2022) e2206851.
[13] B.L. Nguyen, C.D. Phung, D.V. Pham, N.D. Le, J.H. Jeong, J. Kim, J.H. Kim, J. H. Chang, S.G. Jin, H.G. Choi, S.K. Ku, J.O. Kim, Liposomal co-delivery of toll-like receptors 3 and 7 agonists induce a hot triple-negative breast cancer immune environment, J. Control. Release 361 (2023) 443–454.
[14] T.R. Wang, J.F. Ding, S. Liang, Z.Q. Lin, J.X. Yang, Z. Zhang, Z. Zou, G. Li, X. S. Chen, C.L. He, An adhesive immune-stimulating multifunctional hydrogel for potent tumor chemoimmunotherapy and postoperative wound healing promotion, Adv. Funct. Mater. 34 (2024) 2312360.
[15] L.P. Qu, G.H. Cui, Y.P. Sun, R.N. Ye, Y. Sun, F.H. Meng, S.Q. Wang, Z.Y. Zhong, A biomimetic autophagosomes-based nanovaccine boosts anticancer immunity, Adv. Mater. 36 (2024) e2409590.
[16] T. Yamazaki, E. Wennerberg, M. Hensler, A. Buque, J. Kraynak, J. Fucikova, X. K. Zhou, B. Sveinbjornsson, O. Rekdal, S. Demaria, L. Galluzzi, LTX-315-enabled, radiotherapy-boosted immunotherapeutic control of breast cancer by NK cells, Oncoimmunology 10 (2021) 1962592.
[17] N. Furukawa, W.Y. Yang, A.R. Chao, A. Patil, A.C. Mirando, N.B. Pandey, A. S. Popel, Chemokine-derived oncolytic peptide induces immunogenic cancer cell death and significantly suppresses tumor growth, Cell Death Dis. 10 (2024) 161.
[18] M. Motiei, F. Aboutalebi, M. Forouzanfar, K. Dormiani, M.H. Nasr-Esfahani, S. Z. Mirahmadi-Zare, Smart co-delivery of miR-34a and cytotoxic peptides (LTX-315 and melittin) by chitosan based polyelectrolyte nanocarriers for specific cancer cell death induction, Mater. Sci. Eng. C 128 (2021) 112258.
[19] Y. Li, K. Deng, C. Shen, X. Liang, Z. Zeng, L. Liu, X. Xu, Enantiomeric virus-inspired oncolytic particles for efficient antitumor immunotherapy, ACS Nano 17 (2023) 17320–17331.
[20] J. Spicer, A. Marabelle, J.F. Baurain, N.L. Jebsen, D.E. Jossang, A. Awada, R. Kristeleit, D. Loirat, G. Lazaridis, C. Jungels, P. Brunsvig, B. Nicolaisen, A. Saunders, H. Patel, J. Galon, F. Hermitte, K.A. Camilio, B. Mauseth, V. Sundvold, B. Sveinbjornsson, O. Rekdal, Safety, antitumor activity, and T-cell responses in a dose-ranging phase I trial of the oncolytic peptide LTX-315 in patients with solid tumors, Clin. Cancer Res. 27 (2021) 2755–2763.
[21] M. Nielsen, T. Monberg, V. Sundvold, B. Albieri, D. Hovgaard, M.M. Petersen, A. Krarup-Hansen, O. Met, K. Camilio, T. Clancy, R. Stratford, B. Sveinbjornsson, O. Rekdal, N. Junker, I.M. Svane, LTX-315 and adoptive cell therapy using tumor-infiltrating lymphocytes generate tumor specific T cells in patients with metastatic soft tissue sarcoma, Oncoimmunology 13 (2024) 2290900.
[22] H.M. Liu, W. Shen, W.G. Liu, Z.X. Yang, D.K. Yin, C.S. Xiao, From oncolytic peptides to oncolytic polymers: a new paradigm for oncotherapy, Bioact. Mater. 31 (2024) 206–230.
[23] X.Y. Fu, H. Yin, X.T. Chen, J.F. Yao, Y.N. Ma, M. Song, H. Xu, Q.Y. Yu, S.S. Du, Y. K. Qi, K.W. Wang, Three rounds of stability-guided optimization and systematical evaluation of oncolytic peptide LTX-315, J. Med. Chem. 67 (2024) 3885–3908.
[24] Y. Xia, J. Wei, S. Zhao, B. Guo, F. Meng, B. Klumperman, Z. Zhong, Systemic administration of polymersomal oncolytic peptide LTX-315 combining with CpG adjuvant and anti-PD-1 antibody boosts immunotherapy of melanoma, J. Control. Release 336 (2021) 262–273.
[25] C.D. Phung, B.L. Nguyen, J.H. Jeong, J.H. Chang, S.G. Jin, H.G. Choi, S.K. Ku, J. O. Kim, Shaping the "hot" immunogenic tumor microenvironment by nanoparticles co-delivering oncolytic peptide and TGF-β1 siRNA for boosting checkpoint blockade therapy, Bioeng. Transl. Med. 8 (2023) e10392.
[26] B.L. Nguyen, C.D. Phung, D.-V. Pham, N.D. Le, T.O.O. Nguyen, S. Kim, S.G. Jin, H.-G. Choi, J.-H. Chang, C.H. Song, J. Kim, S.K. Ku, J.O. Kim, Reigniting the cancer-immunity cycle with nanoparticles for simultaneous delivery of oncolytic peptides and a TLR agonist, Nano Today 55 (2024) 102179.
[27] J. Yang, R. Zheng, M. Mamuti, D.Y. Hou, Y.D. Zhao, H.W. An, H. Wang, Y. Zhao, Oncolytic peptide nanomachine circumvents chemo resistance of renal cell carcinoma, Biomaterials 284 (2022) 121488.
[28] X. Liu, Y. Zhuang, W. Huang, Z. Wu, Y. Chen, Q. Shan, Y. Zhang, Z. Wu, X. Ding, Z. Qiu, W. Cui, Z. Wang, Interventional hydrogel microsphere vaccine as an immune amplifier for activated antitumour immunity after ablation therapy, Nat. Commun. 14 (2023) 4106.
[29] L. Ye, W. Lv, W. He, S. Li, Z. Min, L. Gong, Q. Zhang, C. Teng, S. Sun, L. Lv, Y. Guo, H. Xin, Reduced malignant glioblastoma recurrence post-resection through the anti-CD47 antibody and temozolomide co-embedded in-situ hydrogel system, J. Control. Release 359 (2023) 224–233.
[30] J. Chen, K. Huang, Q.J. Chen, C. Deng, J. Zhang, Z.Y. Zhong, Tailor-making fluorescent hyaluronic acid microgels via combining microfluidics and photoclick chemistry for sustained and localized delivery of herceptin in tumors, ACS Appl. Mater. Interfaces 10 (2018) 3929–3937.
[31] K. Huang, Y. He, Z. Zhu, J. Guo, G. Wang, C. Deng, Z. Zhong, Small, traceable, endosome-disrupting, and bioresponsive click nanogels fabricated via microfluidics for CD44-targeted cytoplasmic delivery of therapeutic proteins, ACS Appl. Mater. Interfaces 11 (2019) 22171–22180.
[32] Y.H. Long, X.J. Ju, S.H. Yang, S.K. Chen, R. Xie, W. Wang, Z. Liu, D.W. Pan, L. Y. Chu, Microfluidic fabrication of monodisperse hyaluronic acid microspheres with excellent biocompatibility and tunable physicochemical properties, Ind. Eng. Chem. Res. 63 (2024) 6632–6643.
[33] M.Y. He, M.Y. Zhang, T. Xu, S.J. Xue, D.Z. Li, Y.A. Zhao, F. Zhi, D.W. Ding, Enhancing photodynamic immunotherapy by reprograming the immunosuppressive tumor microenvironment with hypoxia relief, J. Control. Release 368 (2024) 233–250.
[34] X.Y. Qiu, Y. Qu, B.B. Guo, H. Zheng, F.H. Meng, Z.Y. Zhong, Micellar paclitaxel boosts ICD and chemo-immunotherapy of metastatic triple negative breast cancer, J. Control. Release 341 (2022) 498–510.
[35] R.D. Song, T.L. Li, J.Y. Ye, F. Sun, B. Hou, M. Saeed, J. Gao, Y.J. Wang, Q.W. Zhu, Z. Xu, H.J. Yu, Acidity-activatable dynamic nanoparticles boosting ferroptotic cell death for immunotherapy of cancer, Adv. Mater. 33 (2021) 2101155.
[36] M. Meng, J.Y. Wu, Y.J. Feng, L. Lin, J. Chen, X. Pang, Y.H. Li, K. Hao, H.Y. Tian, X. S. Chen, A comprehensive strategy based on high clinical translational nanosystem for programmable immunotherapy of triple negative breast cancer, Adv. Mater. 36 (2024) 2314309.
[37] M.S. Barough, A. Seyfoori, E. Askari, M. Mahdavi, R. Sarrami Forooshani, B. Sadeghi, M.H. Kazemi, R. Falak, A. Khademhosseini, N. Mojtabavi, M. Akbari, Gemcitabine-loaded injectable hydrogel for localized breast cancer immunotherapy, Adv. Funct. Mater. 34 (2024) 2403910.
[38] B. Wang, H. Cui, F. Kiessling, T. Lammers, D. Baumjohann, Y. Shi, Targeting intracellular and extracellular receptors with nano-to-macroscale biomaterials to activate immune cells, J. Control. Release 357 (2023) 52–66.
[39] B. Wang, J. Chen, J.S. Caserto, X. Wang, M.L. Ma, An in situ hydrogel-mediated chemo-immunometabolic cancer therapy, Nat. Commun. 13 (2022) 3821.
[40] Z. Zhang, C. He, X. Chen, Designing hydrogels for immunomodulation in cancer therapy and regenerative medicine, Adv. Mater. 36 (2024) 2308894.
[41] A. VanderWalde, S.L. Bellasea, K.L. Kendra, N.I. Khushalani, K.M. Campbell, P. O. Scumpia, L.F. Kuklinski, F. Collichio, J.A. Sosman, A. Ikeguchi, A.I. Victor, T.-G. Truong, B. Chmielowski, D.C. Portnoy, Y. Chen, K. Margolin, C. Bane, C. A. Dasanu, D.B. Johnson, Z. Eroglu, S. Chandra, E. Medina, C.R. Gonzalez, I. Baselga-Carretero, A. Vega-Crespo, I.P. Garcilazo, E. Sharon, S. Hu-Lieskovan, S. P. Patel, K.F. Grossmann, J. Moon, M.C. Wu, A. Ribas, Ipilimumab with or without nivolumab in PD-1 or PD-L1 blockade refractory metastatic melanoma: a randomized phase 2 trial, Nat. Med. 29 (2023) 2278–2285.
[42] J.F. Spicer, A. Marabelle, J.-F. Baurain, A. Awada, R.S. Kristeleit, D.E. Jossang, N. Jebsen, D. Loirat, A.C. Armstrong, G. Curigliano, B. Nicolaisen, O. Rekdal, B. Sveinbjornsson, V.S. Gjerstad, P. Brunsvig, A phase I/II study of the oncolytic peptide LTX-315 combined with checkpoint inhibition generates de novo T-cell responses and clinical benefit in patients with advanced solid tumors, J. Clin. Oncol. 36 (2018) 3094.
[43] J. Sun, Z. Liu, H. Yao, H. Zhang, M. Zheng, N. Shen, J. Cheng, Z. Tang, X. Chen, Azide-masked resiquimod activated by hypoxia for selective tumor therapy, Adv. Mater. 35 (2023) 2207733.
[44] C. Liang, X. Ding, X. Li, X. Jiang, H. Yang, H. Yang, K. Liu, L. Hou, In situ self-reassembling nanosystem enhances PD-L1 blockade for cancer immunotherapy, J. Control. Release 377 (2025) 767–780.
[45] H. Jin, L. Wang, R. Bernards, Rational combinations of targeted cancer therapies: background, advances and challenges, Nat. Rev. Drug Discov. 22 (2023) 213–234.
[46] J. Xie, X. Zhao, P. Zhang, Y. Zhang, R. Cheng, Z. Zhong, C. Deng, Codelivery of BCL2 and MCL1 inhibitors enabled by phenylboronic acid-functionalized polypeptide nanovehicles for synergetic and potent therapy of acute myeloid leukemia, Adv. Sci. 10 (2023) e2204866.
[47] J. Yan, M. Wang, S. Lv, D. Chen, Z. Wu, D. Zhou, S. Zhang, J. Lv, K. Xu, C. Xu, Y. Wei, SiATG5-loaded cancer cell membrane-fused liposomes induced increased uptake of albumin-bound chemotherapeutics by pancreatic cancer cells, J. Control. Release 367 (2024) 620–636.
[48] C.A. Alexander, Y.Y. Yang, Harnessing the combined potential of cancer immunotherapy and nanomedicine: a new paradigm in cancer treatment, Nanomed. Nanotechnol. Biol. Med. 40 (2022) 102492.

[49] Y. Guo, Y. Li, M. Zhang, R. Ma, Y. Wang, X. Weng, J. Zhang, Z. Zhang, X. Chen, W. Yang, Polymeric nanocarrier via metabolism regulation mediates immunogenic cell death with spatiotemporal orchestration for cancer immunotherapy, Nat. Commun. 15 (2024) 8586.
[50] T. Li, B. Li, L. Lin, G. Chen, X. Wang, Y. Chen, W. Huang, M. Cai, X. Shuai, K. Zhu, Anti-CTLA-4 antibody self-presented dendritic cell nanovesicles boost the immunotherapy of hepatocellular carcinoma after microwave ablation, J. Control. Release 376 (2024) 913–929.
[51] M. Babamohamadi, N. Mohammadi, E. Faryadi, M. Haddadi, A. Merati, F. Ghobadinezhad, R. Amirian, Z. Izadi, J. Hadjati, Anti-CTLA-4 nanobody as a promising approach in cancer immunotherapy, Cell Death Dis. 15 (2024) 17.
[52] N. Khranovska, O. Skachkova, O. Gorbach, I. Semchuk, Y. Shvets, I. Komarov, Anticancer immunogenic potential of oncolytic peptides: recent advances and new prospects, Exp. Oncol. 46 (2024) 3–12.
[53] V. Giacco, Long-term results with nivolumab and ipilimumab in melanoma, Nat. Can. 6 (2025) 407.
[54] F.R. Cheng, T. Su, S.R. Zhou, X. Liu, S.L. Yang, S.B. Lin, W.S. Guo, G.Z. Zhu, Single-dose injectable nanovaccine-in-hydrogel for robust immunotherapy of large tumors with abscopal effect, Sci. Adv. 9 (2023) eade6257.
[55] F. Wang, H. Su, Z. Wang, C.F. Anderson, X. Sun, H. Wang, P. Laffont, J. Hanes, H. Cui, Supramolecular filament hydrogel as a universal immunomodulator carrier for immunotherapy combinations, ACS Nano 17 (2023) 10651–10664.
[56] F. Wang, H. Su, D. Xu, M.K. Monroe, C.F. Anderson, W. Zhang, R. Oh, Z. Wang, X. Sun, H. Wang, F. Wan, H. Cui, Therapeutic supramolecular tubustecan hydrogel combined with checkpoint inhibitor elicits immunity to combat cancer, Biomaterials 279 (2021) 121182.
[57] Q. Yu, S. Sun, N. Yang, Z. Pei, Y. Chen, J. Nie, H. Lei, L. Wang, F. Gong, L. Cheng, Self-cascaded pyroptosis-STING initiators for catalytic metalloimmunotherapy, J. Am. Chem. Soc. 147 (2025) 3161–3173.
[58] H. Fang, Y. Wu, L. Chen, Z. Cao, Z. Deng, R. Zhao, L. Zhang, Y. Yang, Z. Liu, Q. Chen, Regulating the obesity-related tumor microenvironment to improve cancer immunotherapy, ACS Nano 17 (2023) 4748–4763.